Journal of ELECTRONIC MATERIALS, Vol. 46, No. 3, 2017
DOI: 10.1007/s11664-016-5173-2

Achieving Low-Electrical-Resistance WO_3:Li Nanostructured Thin Films Using Spray Pyrolysis Technique

ZAHRA ASGHARI[1] and HOSEIN ESHGHI[1,2]

1.—Department of Physics, Shahrood University of Technology, Shahrood, Iran. 2.—e-mail: h_eshghi@shahroodut.ac.ir

We have grown 1 wt.%, 5 wt.%, and 10 wt.% Li-doped tungsten oxide thin films on glass substrate using the spray pyrolysis technique and investigated their morphological, structural, optical, and electrical properties. In addition to formation of nanograin coverage, we found that the doped films grew with polycrystalline monoclinic structure having preferred orientation along (200) plane instead of the amorphous undoped structure. The 10 wt.%-doped sample showed the highest visible transmittance (~95%) and lowest resistivity (~7.5 Ω cm), together with relatively high ultraviolet (UV) photoluminescence emission at room temperature.

Key words: WO_3:Li, thin films, nanostructure, spray pyrolysis, electrical and optical properties

INTRODUCTION

Among transition-metal oxides, tungsten oxide is an *n*-type semiconductor with indirect bandgap in the range from 2.4 eV to 3.7 eV, depending on the growth conditions used.[1,2] Grown samples may contain various crystalline phases such as WO_3, WO_2, WO_{3-x}, etc. Researchers have identified various applications for tungsten oxide thin films depending on their electrochromic, optochromic, and photocatalytic properties, including flat-panel displays, smart windows, decorative glasses, and H_2, H_2S, NH_3, and NO_x gas sensors.[3,4]

To date, researchers have studied the effect of different dopants such as Li,[5,6] TiO_2,[7,8] Pt,[9,10] C,[11] Cu,[12] Na, N_2, Ag, and Au[13–16] on the physical properties of WO_3 thin films.

A number of techniques including sputtering,[17] thermal evaporation,[18,19] the sol–gel method,[19] and spray pyrolysis[20,21] have been used to grow this material. Among these, spray pyrolysis has attracted more attention due to its advantages such as short deposition time, simple technology, low cost, no need for vacuum, and relatively good adhesion to the substrate. In this study, the effects of Li doping on the physical properties of WO_3 thin films grown on glass substrate using the spray pyrolysis technique were investigated.

(Received July 4, 2016; accepted November 21, 2016; published online December 9, 2016)

EXPERIMENTAL PROCEDURES

Before deposition, the substrates were washed with soap and water, then placed in acetone and distilled water in an ultrasonic machine for 16 min. Finally, samples were washed with ionized water and dried with nitrogen gas.

Ammonium tungstate solution $(NH_4)_2WO_4$ (50 ml) was made from pure (99.9%) WO_3 powder in ammonia and distilled water. For Li doping, we used LiCl powder as source material, dissolved in 50 ml $(NH_4)_2WO_4$ solution at 0 wt.%, 1 wt.%, 5 wt.%, and 10 wt.% (labeled as PW, W1L, W5L, and W10L, respectively). Finally, the solution was sprayed onto glass substrates at 400°C. We expected that WO_3 thin-layer deposition would follow the chemical reactions in Eqs. 1 and 2[22]:

$$WO_3 + 2NH_3 + H_2O \rightarrow (NH_4)_2WO_4 \quad (1)$$

$$(NH_4)_2WO_4 \rightarrow WO_3 + H_2O + 2NH_3 \quad (2)$$

Sample morphology was investigated by field-emission scanning electron microscopy (FESEM, S.4160 model). Structural characterization of the films was carried out by x-ray diffraction analysis

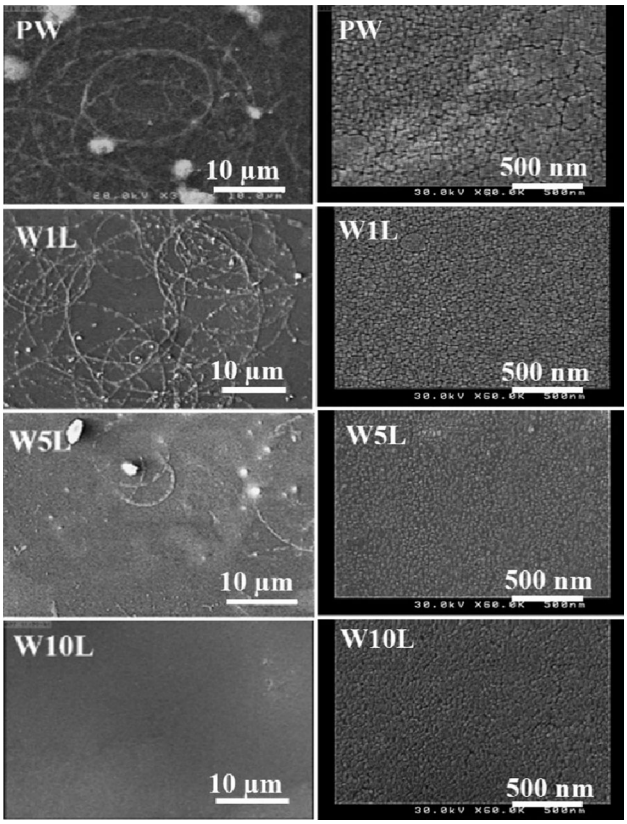

Fig. 1. FESEM images of pure and Li-doped WO_3 samples.

with Cu K_α radiation (wavelength 1.54 Å) in the 2θ angle range from 10° to 70° (XRD; Bruker AXS). To study their optical properties, the photoluminescence (PL) spectrum of the samples was measured at room temperature using a fluorescence spectrophotometer (Cary Eclipse) including a xenon arc lamp with excitation wavelength of 253 nm. We measured the transmittance spectrum of the samples using an ultraviolet–visible (UV–Vis) spectrophotometer (Shimadzu 1800) in the wavelength range from 300 nm to 1100 nm. Thickness was measured using a Taylor Hobson profilometer with accuracy of ±20 nm.

RESULTS AND DISCUSSION

Surface Morphology

Figure 1 shows FESEM images of the grown samples. The pure sample was covered with a number of flat thin layers, forming spiral strings with diameter of about 300 nm or less. As the doping concentration was gradually increased, the diameter of the strings reduced, and they finally all disappeared. In addition, according to the FESEM images at 500 nm scale, the area between the strings was covered with relatively uniform nanosized grains with diameter less than ~30 nm, which gradually decreased as the doping concentration was increased.

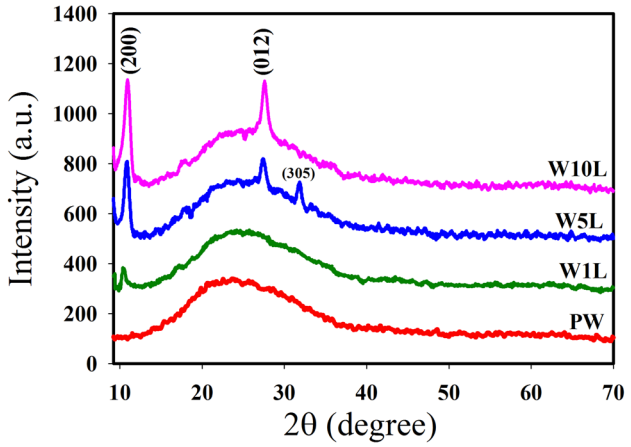

Fig. 2. XRD spectra of pure and Li-doped samples.

Structural Properties

Figure 2 shows the XRD patterns of the layers. It is notable that none of the samples showed phases other than tungsten oxide. According to these results, although the pure sample (PW) was amorphous, the doped ones showed polycrystalline monoclinic structure with lattice parameters of a = 18.28 Å, b = 3.77 Å, and c = 13.98 Å [Joint Committee on Powder Diffraction Standards (JCPDS) 05-0392]. According to these spectra, all the doped samples mainly grew along (200) direction, with corresponding Bragg angle of ~12°. With increasing doping concentration, the relative intensity of the diffraction peaks gradually increased, indicating higher film quality. This can be explained based on the fact that, although it is expected that addition of an impurity to a crystalline solid will tend to introduce disorder into the material, this is true only if the impurities are located interstitially (between lattice points) rather than occupying exact lattice sites. Only under certain growth conditions is it possible for the impurity mainly to substitute at exact lattice sites. Under such conditions, the atomic planes will be ordered and the film quality will tend to improve.

Using crystalline structure theory, one can deduce the distance between adjacent planes and the crystallite size of the grown samples.

Distance Between Crystal Planes $d_{(hkl)}$

This quantity can be obtained from Bragg's relation,

$$d_{(hkl)} = \lambda/2\sin\theta \qquad (3)$$

Our calculations showed that, for the doped samples, $d_{(200)}$ was 0.8238 nm, 0.8194 nm, and 0.8108 nm, respectively.

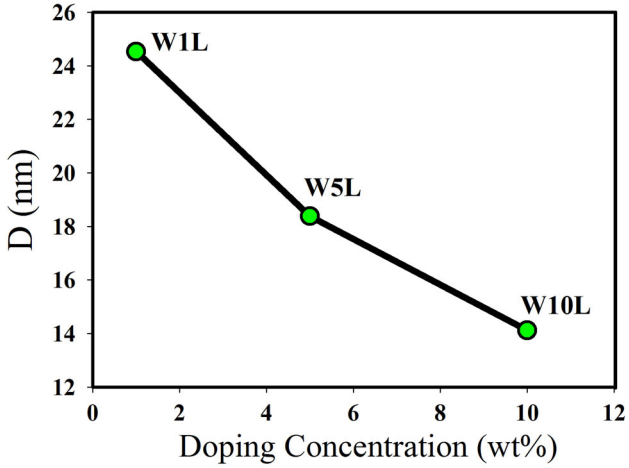

Fig. 3. Variation of crystallite size in studied WO_3:Li samples.

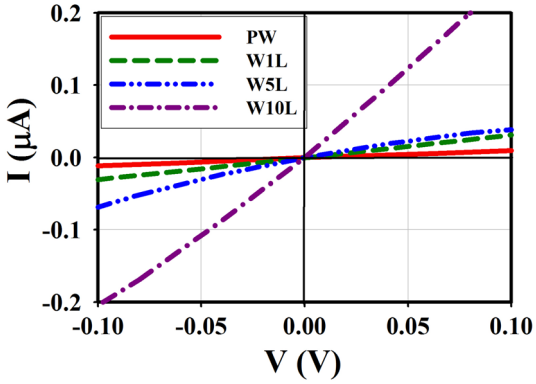

Fig. 4. *I–V* curves of the studied samples.

Crystallite Size (D)

The crystallite size corresponding to a given Bragg angle θ can be found using Scherrer's equation,

$$D = 0.9\lambda/\beta\cos\theta, \quad (4)$$

where λ is the x-ray wavelength and β is the full-width at half-maximum (FWHM) of the given peak. The results of these calculations are shown in Fig. 3. It is clear that, with increasing doping concentration, the crystallite size reduced from 24.53 nm ± 0.01 nm to 14.12 nm ± 0.01 nm.

Electric and Thermoelectric Properties

Figure 4 shows the current–voltage curves of the pure and Li-doped samples.

All samples showed an ohmic characteristic, with the resistivity of the layer reducing with increasing doping level. Considering the equations for the sheet resistance ($R_s = \frac{V}{I}$) and layer resistivity ($\rho = R_s t$ where t is the thickness of the layer), we measured these quantities on 1 cm × 1 cm samples. The variation of the resistivity of the layers is shown in

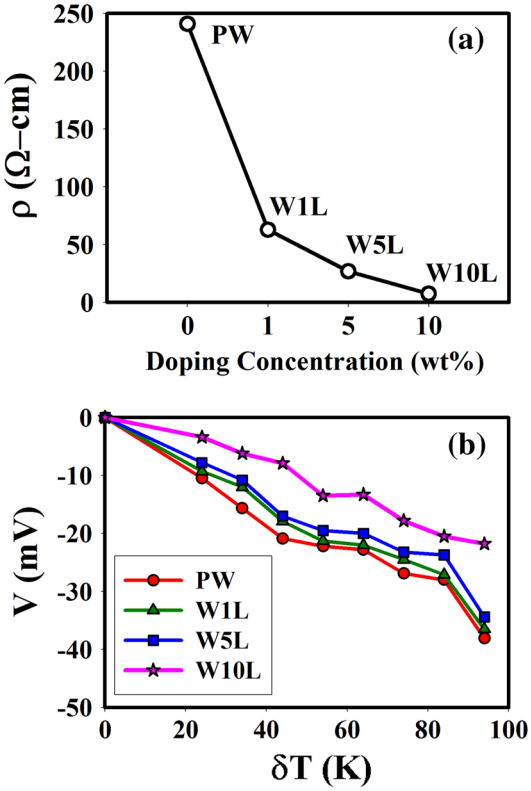

Fig. 5. (a) Electrical resistivity and (b) Seebeck effect results for pure and Li-doped samples.

Fig. 5a. According to these results, the film resistivity decreased sharply from 241.0 nm ± 0.5 Ω cm for PW to 60.0 nm ± 0.5 Ω cm for W1L, then gradually to 7.5 Ω cm ± 0.5 Ω cm for the W10L sample, the lowest reported value for WO_3:Li grown by the spray pyrolysis method. This can be attributed to the fact that the Li atoms were correctly located at WO_3 lattice sites, especially oxygen vacancy (V_O) sites. Such replacement can lead to formation of donor levels instead of donor-like localized defect states close to the conduction-band edge (CBE), playing the role of donor atoms in the material.[24,25] The Seebeck effect results (Fig. 5b) confirmed the *n*-type conductivity of the samples, as also reported by other researchers.[25,27,28]

Optical Properties

UV–Vis Spectra

Figure 6 shows the UV–Vis transmission spectra for the studied samples. It is clear that, as the doping concentration was increased, the transmission of the layers increased, from about 80% for the undoped sample to almost 95% for the doped layers. Similar behavior was reported by Kovendhan[5] and Chacko et al.[26] This variation may be due to both the reduction in the sample thickness (from 250 nm for PW to 190 nm, 210 nm, and 180 nm for the

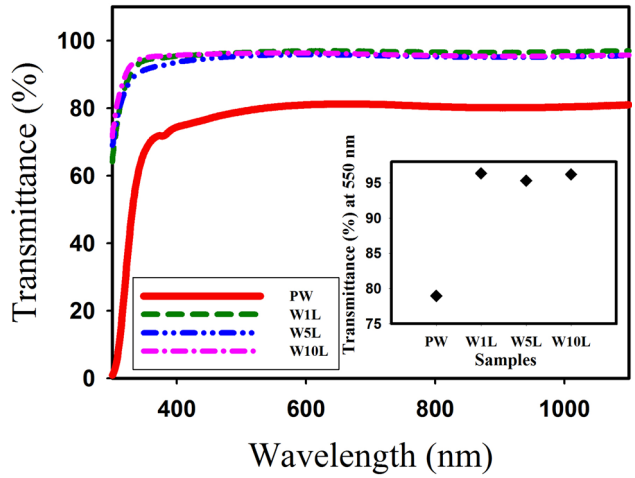

Fig. 6. Transmittance spectra of undoped and Li-doped WO_3 films. Inset shows the transmittance of the layers at 550 nm.

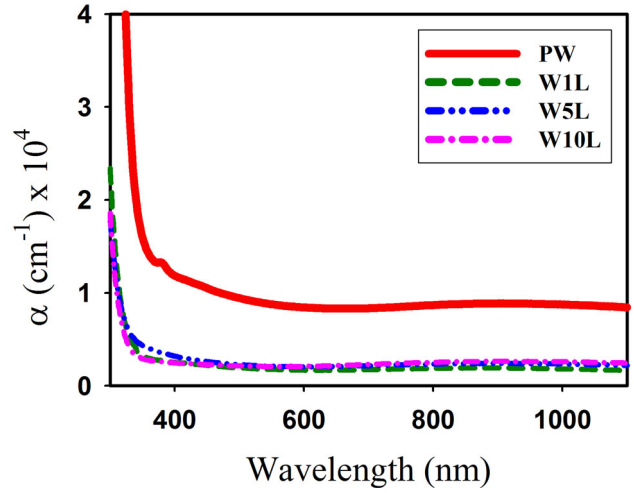

Fig. 7. Absorption coefficient versus wavelength for the studied samples.

doped samples, respectively) as well as the improved crystallinity of the doped samples (Fig. 2).

Figure 7 shows the absorption coefficient spectra for the studied samples as a function of wavelength, obtained using the Lambert equation,

$$\alpha = \frac{-\ln T}{t}, \tag{5}$$

where t is the thickness of the layer.

These results indicate that the samples had relatively high absorption coefficient ($\sim 10^4$ cm^{-1}) in the ultraviolet region ($\lambda < 400$ nm). According to these data, the PW sample had a very sharp absorption edge at 320 nm, and with increasing Li concentration, the absorption edge shifted towards shorter wavelength. Using these data, we found the optical bandgap, E_g, of the studied films using the relation[23]

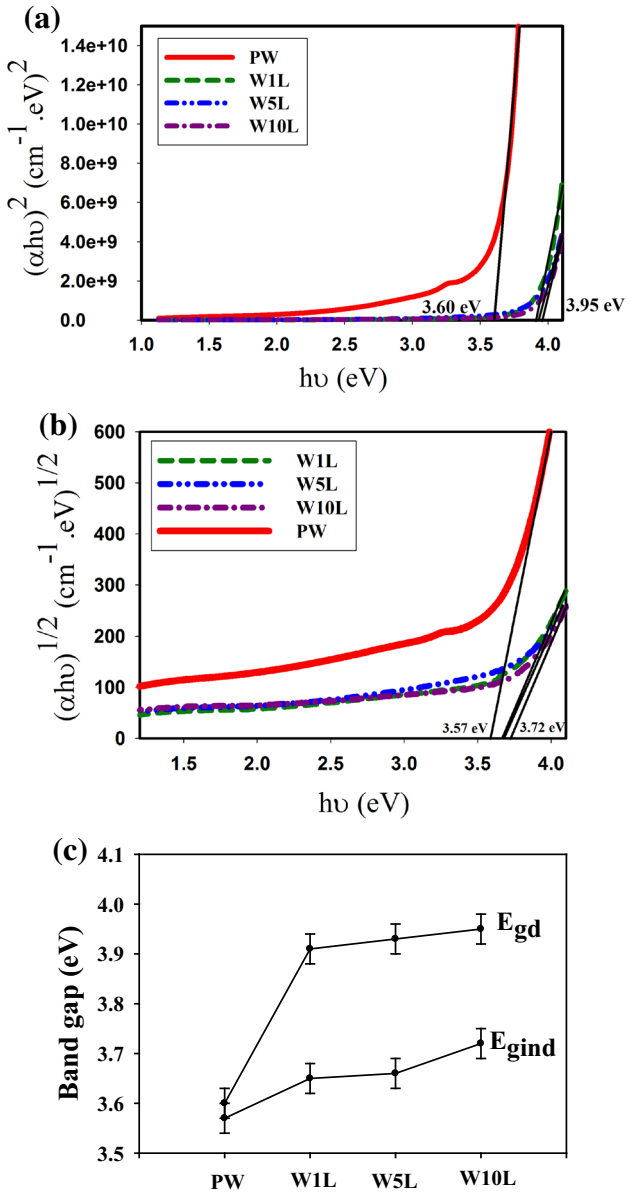

Fig. 8. Details of bandgap determination: (a) direct and (b) indirect bandgaps, and (c) final calculated results and variations of E_{gd} and E_{gind} (error bars show the uncertainty on the evaluated bandgaps).

$$(\alpha h\upsilon)^m = A(h\upsilon - E_g), \tag{6}$$

where A is a constant, $h\upsilon$ is the incident photon energy, and m depends on the nature of the band transition ($m = 2$ for direct, $m = 1/2$ for indirect). Direct and indirect bandgaps can be determined by extrapolation of the straight-line portion to the energy axis, i.e., $(\alpha h\upsilon)^m = 0$. The details of our analysis for the direct and indirect bandgaps are shown in Fig. 8a and b, and the final results in Fig. 8c.

According to these results, E_{gd} increased from 3.60 eV to 3.95 eV and E_{gind} from 3.57 eV to 3.72 eV as the doping concentration was increased. In

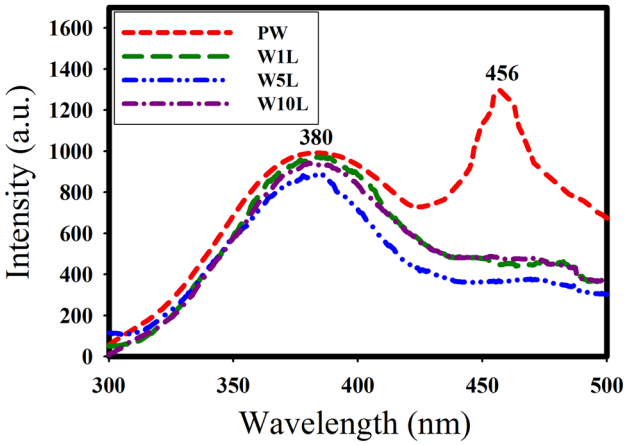

Fig. 9. PL spectra of undoped and Li-doped WO_3 samples.

addition, one can see that: (a) for all the samples, $E_{gind} < E_{gd}$, indicating that the WO_3 thin layers had indirect bandgap nature; and (b) the positive slope in the variations of E_{gind} and E_{gd} for the doped samples can be ascribed to the quantum confinement effect, according to which the bandgap of a semiconductor depends on the crystal size, increasing with decreasing grain and crystallite sizes. This is compatible with the data shown in Fig. 3.

Photoluminescence Spectra

Figure 9 shows the PL spectra of the grown samples, in spite of the indirect bandgap nature of the material. The data for the undoped sample show two clear peaks, one at 380 nm (3.26 eV) in the invisible UV region, and another at 456 nm (2.7 eV), in the visible region. These peaks can be attributed to band–band transitions, and the presence of localized states in the bandgap, which is related to crystalline defects.[1,9] These data also indicate that, for the doped samples, the visible peak intensity was drastically reduced. The relative decline of this peak could be a sign of reduced crystal defects, as confirmed by the electrical and optical properties of these layers.

CONCLUSIONS

Nanostructured thin films of undoped and 1 wt.%, 5 wt.%, and 10 wt.% Li-doped WO_3 were deposited on glass substrates using the spray pyrolysis technique. It was found that doping improved the crystallinity, increasing not only the optical transmission but also the electrical conductivity (to ~95% and ~7.5 Ω cm for the W10L sample, respectively). Such improvement can be attributed to reduced crystal defects, mainly oxygen vacancies, in the material, as also confirmed by the electrical and optical properties including the variation of the optical bandgap and PL spectrum.

REFERENCES

1. Y.T. Heieh and M.W. Huang, *Thin Solid Films* 519, 1668 (2010).
2. B. Cole, B. Marsen, E. Miller, Y. Yan, B. To, K. Jones, and M. Al-Jassim, *J. Phys. Chem. C* 112, 5213 (2008).
3. C.G. Granqvist, *Sol. Energy Mater. Sol. Cells* 60, 201 (2000).
4. C. Sella, M. Maaza, O. Nemraoui, J. Lafait, N. Renard, and Y. Sampeur, *Surf. Coat. Technol.* 98, 1477 (1998).
5. M. Kovendhan, D. Paul Joseph, E. Senthil Kumar, A. Sendilkumar, P. Manimuthu, S. Sambasivam, C. Venkateswaran, and R. Mohan. *Appl. Surface Sci.* 257, 8127 (2011).
6. I. Porqueras and E. Betran, *Thin Solid Films* 377, 129 (2000).
7. J. Livahe and G. Guzman, *Solid State Ionics* 84, 205 (1996).
8. J. Wang, J.M. Bell, and I.L. Skryabin, *Sol. Energy Mater. Sol. Cell* 56, 465 (1999).
9. R. Abe, H. Takami, N. Murakami, and B. Ohtani, *J. Am. Chem. Soc.* 130, 7780 (2008).
10. M. Qamar, M.A. Gondal, and Z.H. Yamani, *Catal. Commun.* 11, 768 (2010).
11. Y. Sun, C.J. Murphy, K.R. Reyes-Gil, E.A. Reyes-Garcia, J.M. Thornton, N.A. Morris, and D. Raftery, *Int. J. Hydrogen Energy* 34, 8476 (2009).
12. H. Widiyandari, A. Purwanto, R. Balgis, T. Ogi, and K. Okuyama, *Chem. Eng. J.* 180, 323 (2012).
13. A. Shengelaya, S. Reich, Y. Tsabba, and K.A. Muller, *Eur. Phys. J. B* 12, 13 (1998).
14. D. Paluselli, B. Marsen, E.L. Miller, and R.E. Rocheleau, *Electrochem. Solid State Lett.* 8, G301 (2005).
15. S.M. Sun, W.Z. Wang, S.Z. Zeng, M. Shang, and L. Zhang, *J. Hazard. Mater.* 178, 427 (2010).
16. P.M. Kadama, N.L. Tarwale, P.S. Shindee, S.S. Malie, R.S. Patil, A.K. Bhosalec, H.P. Deshmukhd, and P.S. Patil, *J. Alloys Compd.* 509, 1729 (2011).
17. D. Ronnow, D. Kullman, and C.G. Granqvist, *J. Appl. Phys.* 80, 423 (1996).
18. L. Lozzi, L. Ottaviano, M. Passacantando, S. Santucci, and C. Cantalini, *Thin Solid Films* 391, 224 (2001).
19. C. Cantalini, W. Wlodarski, Y. Li, M. Passacantando, S. Santucci, E. Comini, G. Faglia, and G. Sberveglieri, *Sens. Actuators B* 64, 182 (2000).
20. M. Regragui, M. Addou, A. Outzourhit, E. El Idrissi, A. Kachouane, and A. Bougrine, *Sol. Energy Mater. Sol. Cells* 77, 341 (2003).
21. M. Regragui, M. Addou, A. Outzourhit, J.C. Bernede, E. El Idrissi, E. Benseddik, and A. Kachouane, *Thin Solid Films* 358, 40 (2000).
22. R. Sivakumar, A.E.R. Moses, B. Subramanian, M. Jayachandran, D.C. Trivedi, and C. Sanjeeviraja, *Mater. Res. Bull.* 39, 1479 (2004).
23. S.R. Bathe and P.S. Patil, *Solar Energy Mater. Solar Cells* 91, 1097 (2007).
24. L.M. Bertus, A. Enesca, and A. Duta, *Thin Solid Films* 520, 4282 (2012).
25. M. Regragui, M. Addou, A. Outzourhit, E. El Idrissi, A. Kachouane, and A. Bougrine, *Solar Energy Mater. Solar Cells* 77, 341 (2003).
26. S. Chacko, M.J. Bushiri, and V.K. Vaidyan, *J. Phys. D Appl. Phys.* 39, 4540 (2006).
27. P.S. Patila, P.R. Patilb, and E.A. Ennaouic, *Thin Solid Films* 370, 38 (2000).
28. M. Gilleta, K. Aguira, C. Lemirea, E. Gilleta, and K. Schierbaumb, *Thin Solid Films* 467, 239 (2004).